

# A Study of Transformer Winding Vibration using a Laser Doppler Vibrometer

Jing Zheng<sup>1,2</sup>, Jie Pan<sup>1</sup> and Hai Huang<sup>2</sup>

(1) School of Mechanical and Chemical Engineering, The University of Western Australia, WA 6009

(2) Department of Instrument Science and Engineering, Zhejiang University, China

## ABSTRACT

Many reported transformer failures are due to failures in the windings. Investigation of the behaviours of windings under different failure modes has become a focus for research into fault diagnosis of power transformer windings. In this paper, a laser Doppler vibrometer (LDV) is used to study the winding vibration of a single-phase disk-type power transformer with various causes of failure, such as loosening of winding clamping pressure and removal of insulation blocks on the winding. The results demonstrate that these causes can be identified and characterized by the pattern of surface velocities due to winding vibration. The winding's vibration pattern displays a significant change as the winding clamping pressure gradually decreases. Missing or shifting insulation blocks often lead to a rise in winding vibration and a change in the vibration pattern. The obtained spatial distribution of transformer winding vibration is useful for understanding the details of transformer vibration and for future study of the interaction between the winding and the transformer tank.

## INTRODUCTION

Transformers are vital components in power network infrastructure, and the failure of transformers may directly and indirectly cause considerable economic losses, in addition to adversely affecting network reliability. The increasing availability of on-line monitoring and diagnosis systems can assist in detecting potentially damaging faults in transformers early enough to take appropriate actions (Lord and Hodge, 2010).

The vibration-based method for monitoring and fault diagnosis in a transformer is a relatively new technique. The main source of transformer vibration is the transformer's active part (Bagheri and Naderi, 2011), which consists of the transformer core and winding. The magnetostrictive and electrodynamic forces induce vibrations on the core and winding, respectively. Then the vibration from the active part propagates through the mechanical joints and transformer oil to the tank walls (Berler, et al, 2000). Thus the health condition of the active part can be efficiently assessed by using the vibration signature of the transformer tank (Nafar, Bahmanifrouzi and Jabbari, 2011).

In order to understand the generation, transmission and superposition of transformer vibrations, several experimental studies have been performed, with transducers placed on the windings and core (Boczar and Borucki, 2008). However, a comparison with the measured data on the transformer tank indicated that only a few points on the tank had a vibration that showed a good correlation with the winding and core vibrations. Therefore, to establish a link between the internal and external vibrations of the transformer, detailed measurements of winding and core vibration are necessary.

Transducers have been utilized as vibration collectors in traditional vibration measurements. However, the following factors indicate that a transducer is not suitable for the measurement of internal vibration:

- (1) In walk-around monitoring of power transformers, magnetic mounts are normally used for conven-

ience. Magnetic mounts are available with flat surfaces for flat locations. However, on a rough surface, such as the winding, magnetic mounts require additional materials, which will affect mounting resonance and the typical usable frequency ranges of transducers. Grounding and shielding techniques are also required for magnetic mounts to avoid unpredictable errors caused by electromagnetic interference, especially within a running transformer.

- (2) When a large number of measuring points are desired, the application of traditional transducers becomes prohibitively expensive and labour-intensive, if not impossible.

With regards to the problems mentioned above, a laser is a good alternative to the traditional transducer. A laser Doppler vibrometer (LDV) is a scientific instrument that is used to make non-contact vibration measurements of a surface. The laser beam from the LDV is directed at the measuring position on the surface, and the vibration amplitude and frequency are extracted from the Doppler shift of the laser beam's frequency due to the motion of the surface. Because of the non-contact measurement of vibration, the error introduced by mounting techniques is eliminated. As the laser can scan over the plane of an object, a measurement of the active part of a transformer with a large number of measuring points can be realized.

Few detailed internal measurements of transformer vibration have been conducted. Mizokami (Mizokami, Yabumoto and Okazaki, 2005) developed a laser-based vibration measurement system. He applied the system to a three-phase three-limb transformer core, in order to examine the vibration pattern of a transformer core under a normal steady-state condition.

In this paper, measurements have been performed on a single-phase transformer winding using a non-contact LDV. The vibration pattern of the transformer winding is also investigated, not only in healthy conditions, but also when the winding is set in artificially faulty conditions.

### MEASUREMENT SCHEME

The object to be measured is the active part of a single-phase 1 kVA model transformer (Figure 1), located at the School of Mechanical and Chemical Engineering of the University of Western Australia.



Figure 1: The UWA model transformer.

The results obtained in this paper are based on an analysis of vibration data collected by the measurement system shown in Figure 2. Vibrations of the transformer winding, both with and without faults, were measured with an LDV. To acquire a refined and detailed vibration pattern of the transformer winding, the scanning points should cover the surface of one side of the winding. In laser coordinates, 11×11 scanning points on one side of the winding surface were selected for measurement (Figure 3). The horizontal distance between the scanning points was approximately 1.6 cm, and the vertical distance was about 2 cm, which is nearly twice the thickness of the winding disk. Moreover, 130 additional points were arranged on the core for comparison purposes.

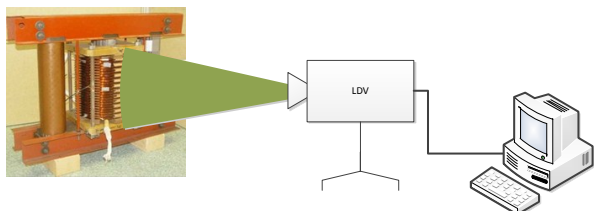


Figure 2: The measurement system.

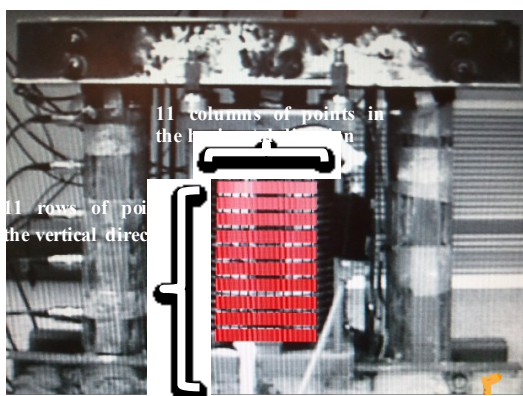


Figure 3: The arrangement of scanning points on the winding.

The measurements included recording the radial vibrations of winding under the following three conditions:

- (1) Case 0: Winding vibrations were due to steady-state electrical excitation and the settings of the

winding's clamping pressure and insulation blocks were all at normal operating conditions.

- (2) Cases 1–36: The winding clamping pressure was created by tightening the winding clamping bolts (as shown in Figure 4). A perfectly pre-compressed winding was provided with adequate strength to withstand a short-circuit's mechanical force. As a result, loosening the bolted joints on the winding decreased the clamping force under the bolt heads, and correspondingly introduced potential mechanical defects into winding. Case 1 to Case 36 corresponded to the winding vibration with slackened clamping bolts on the winding (which gave rise to a reduced winding clamping pressure); the number indicates the degree of slackness. The clamping bolts were designed to be loosened (counter-clockwise/left) by an angular displacement of  $i \times 22.5^\circ$  for each case, where  $i$  is the index number of the case and  $i \in (1, 2, \dots$
- (3) Cases 1'–4': Insulation failure has been considered as one of the major causes of failure of power transformers (Dey and Chakravorti, 2011). Excessive overloads by an impulse voltage may cause insulation deterioration, a loose connection or a breakdown of transformer insulation (Oliveira and Cardoso, 2010). In order to study the vibration behaviour of windings under the failure mode of insulation deterioration, four insulation blocks (Figure 4(b)) were removed from the winding one by one as noted by Cases 1' to 4' of the vibration measurements.

All of the vibration measurements were performed while the supply voltage was the transformer's rated voltage, while the secondary winding of the transformer was left open-circuited

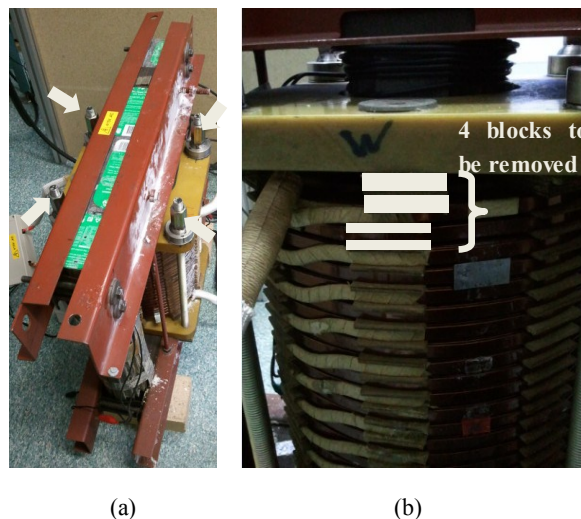


Figure 4: Images of (a) winding clamping bolts and (b) insulation blocks.

### RESULTS AND DISCUSSION

The analysis of the winding vibration was conducted in the frequency domain by application of a Fast Fourier Transform (FFT). The FFT spectrum of the vibration at one scanning point ( $n, m$ ) on the winding is given by  $S_{n,m}$ , where  $n$  is the row index number (increasing from left to right) and  $m$  is the column index number (increasing from bottom to top). Since

there are 11×11 scanning points on the winding, a spatial matrix of the winding vibration spectrum is described by:

$$S(f) = \begin{bmatrix} s_{1,1}(f) & \dots & f \\ \vdots & \ddots & \vdots \\ s_{11,1}(f) & \dots & f \end{bmatrix}, \quad (1)$$

which describes the winding vibration pattern or spatial distribution at frequency  $f$ .

**Case 0**

When the transformer is running under normal operating conditions, the vibration of the transformer winding depends on the current squared. The current, for either the secondary loaded or unloaded configurations, had a dominating 50 Hz component. As a result, 100 Hz was regarded as the main harmonic of winding vibration, as demonstrated by the averaged FFT spectrum  $\bar{s}$  shown in Figure 5. Here, the spatial averaged FFT spectrum of winding vibration is calculated by:

$$\bar{s}(f) = \frac{\sum_{n=1}^{11} \sum_{m=1}^{11} s_{n,m}(f)}{11 \times 11}. \quad (2)$$

The averaged spectrum also shows other harmonics at multiples of 50 Hz, due to the distortion of the magnetizing current or some residual harmonic currents (Bel'en and Juan, 2005).

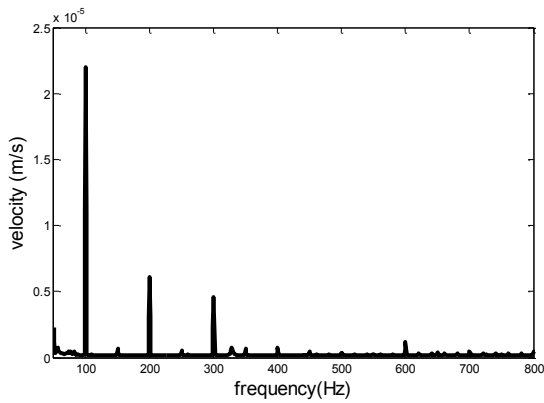


**Figure 5:** Averaged FFT spectrum of winding vibration for Case 0.

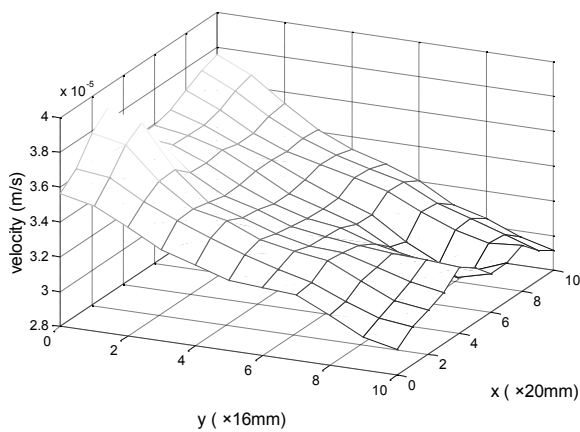


**Figure 6:** RMS velocity pattern of winding vibration for Case 0.

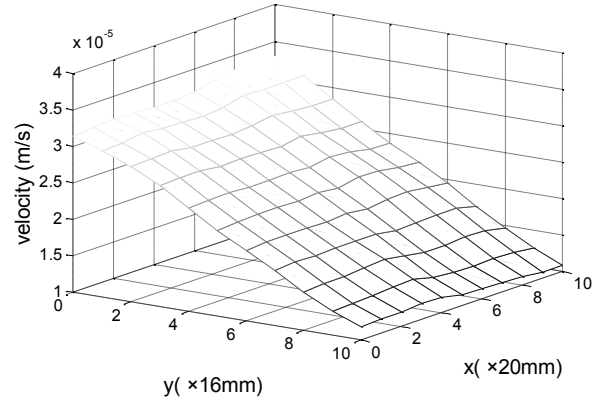


**Figure 7:** The 100 Hz velocity pattern of winding vibration for Case 0.

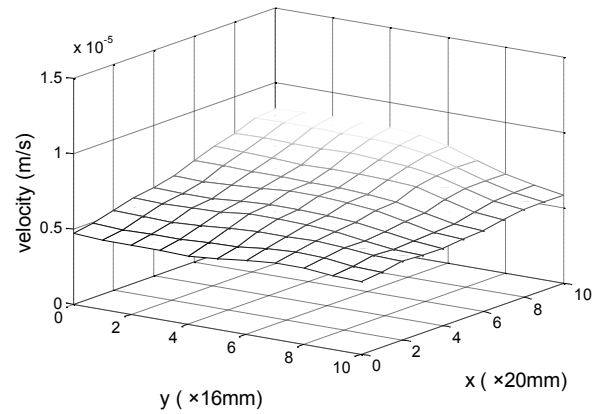


**Figure 8:** The 200 Hz velocity pattern of winding vibration for Case 0.

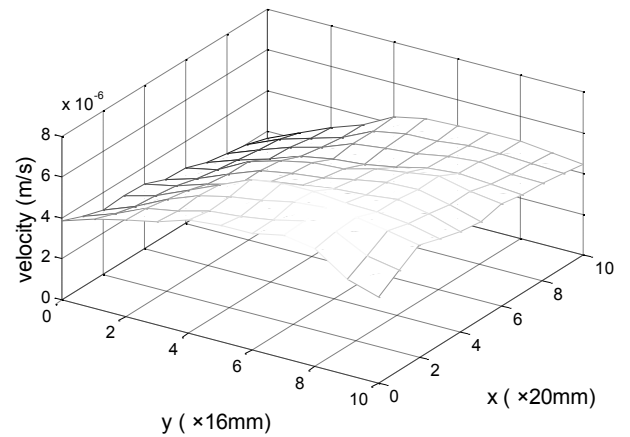


**Figure 9:** The 300 Hz velocity pattern of winding vibration for Case 0.

The root-mean-square (RMS) velocity for all points is presented by a 3D plot (see Figure 6). The  $x$  and  $y$  coordinates are the indices of the scanning points in the horizontal and vertical directions, respectively, and the number 0 is defined as the leftmost/lowermost point on the winding. The  $z$  coordinate represents the winding vibration velocity. The vibration energy is apparently spatially distributed across the entire surface of the winding, and is attributed to the spatial velocity fluctuation of each frequency component. The spec-

tra  $S(100)$ ,  $S(200)$  and  $S(300)$  are plotted in Figures 7, 8 and 9, respectively. The  $S(100)$  plot is significant and impressive, with approximate bilateral (left–right) symmetry across the horizontal axis, and an apparently linear decrease along the vertical axis.

**Cases 1 to 36**

Figures 10–14 show the velocity patterns of winding vibration at 100 Hz for the 37 cases, where clamping bolts were turned by different amounts in the loosening direction to selectively obtain different predetermined amounts of clamping force. In each case, the clamping bolts were designed to be loosened by  $i \times 22.5^\circ$  ( $i$  is the index number of each case,  $i \in (1, 2, \dots)$ ).

As Figure 10 shows, when the winding clamping bolts are sufficiently or properly tightened (Cases 1–4), the spatial vibration distribution always follows a pattern like that of Case 0 (Figure 7). However, the vibration amplitudes fluctuate with the change in clamping force on certain parts of the winding. That is to say, the vibration measurements are sensitive enough to detect the structural changes, even slight ones.

Structural looseness may cause increased winding vibration. The stiffness of the structure changes as the looseness increases. When the clamping force becomes severely loose, the winding vibrations grow in intensity, as shown in Figure 12.

For the early stages of looseness (Cases 6 to 10), significant changes occur at the bottom end of the winding, as shown in Figure 11. In the secondary stage, the four clamping bolts were loosened by more than 5/8ths of a turn. However, deviation among the clamping forces created by the four bolts will be introduced by the mounting procedure, since it is difficult to make each bolt turn an exactly equal amount. This clamping force deviation gives rise to the imbalance and asymmetry of the structural stiffness, which leads to an obvious and non-negligible effect on the vibration pattern. In Figure 12, the vibration amplitude, not only in the lower left part but also in the upper right part, is increased dramatically with as the looseness increases in severity, leaving the velocity pattern highly asymmetrical and very different from that of Case 0. In the tertiary stage (Cases 22 to 28), the clamping forces created by the four bolts gradually approached zero, as did the deviation. Figures 13(a)–(e) indicate that the velocity pattern varied dramatically in this stage, gradually adjusting to a shape of symmetry and balance, resembling the patterns in Figure 14. In the final stage, the winding bolts have been almost completely loosened. What is most remarkable is that the velocity pattern has been thoroughly inverted from that of Case 0. In particular, Figure 14 indicates that vibration amplitudes at the bottom part of the winding are excessively large, nearly 1.5 times that of the top part.

Moreover, looseness of the clamping force also brings about an impressive change in the velocity pattern of vibration at other frequency components, such as  $S(200)$  and  $S(300)$ . As presented in Figure 15, the vibration at all scanning points for 200 Hz is generally of equal amplitude, and undergoes a slight rise as a result of a modest loss of clamping force, due to the decrease in structure stiffness. Conspicuous changes induced by increasing looseness can be found in Figure 16. The middle part, in particular, experiences a surge in velocity. Ultimately, the velocity pattern at 200 Hz is converted to a shape that is extremely similar to that of 100 Hz, with much higher amplitudes in the lower part.

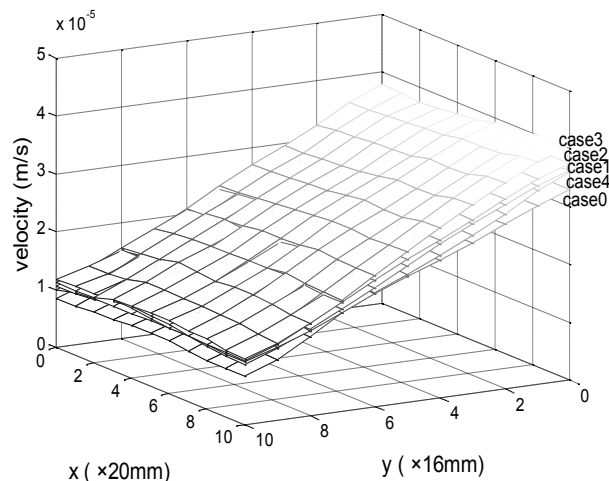


**Figure 10:** Vibration distribution on the winding at 100 Hz for totally tight and generally tight cases, Cases 0–4.

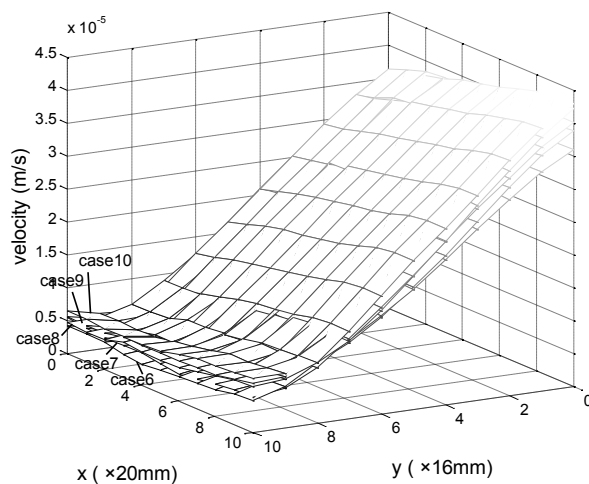


**Figure 11:** Vibration distribution on the winding at 100 Hz for slightly loosened clamping pressures, Cases 6–10.

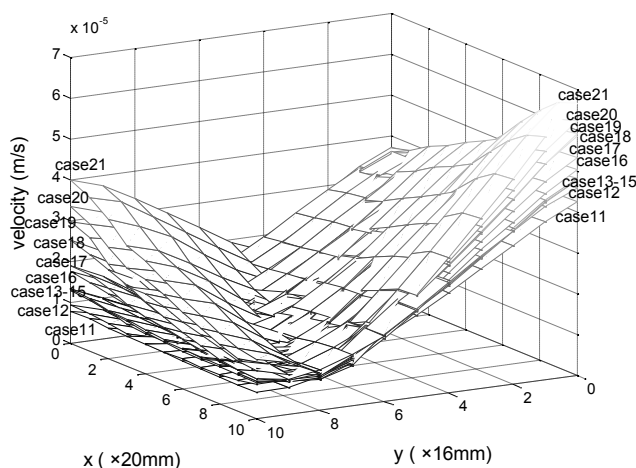
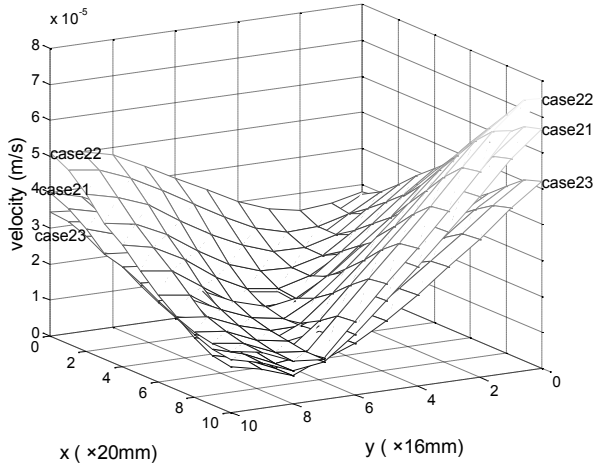
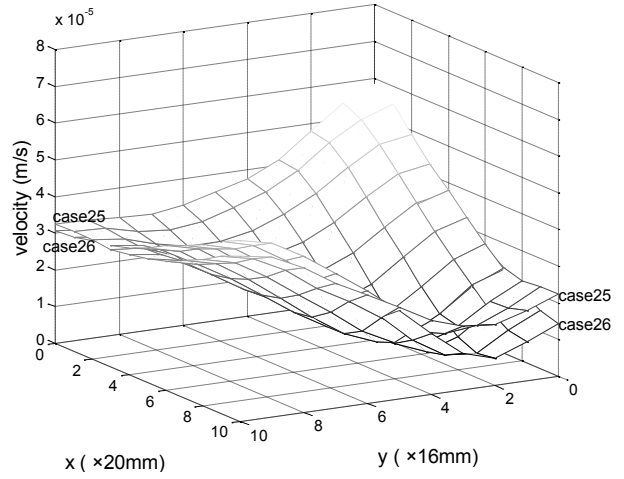


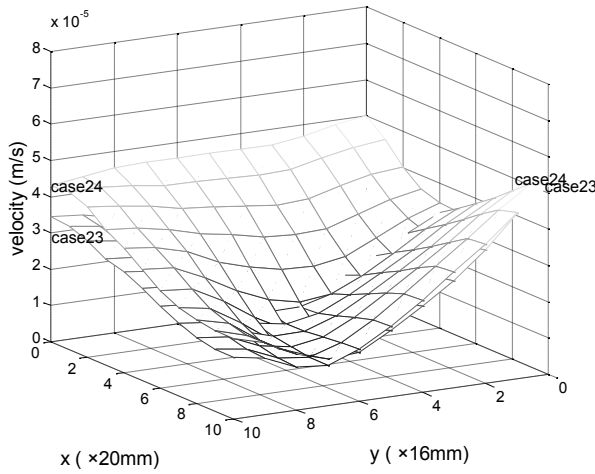
**Figure 12:** Vibration distribution on the winding at 100 Hz for generally loosened cases, Cases 11–21.



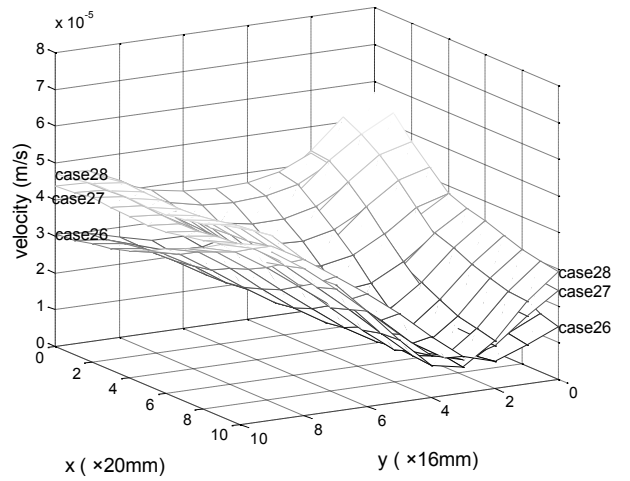
(a)



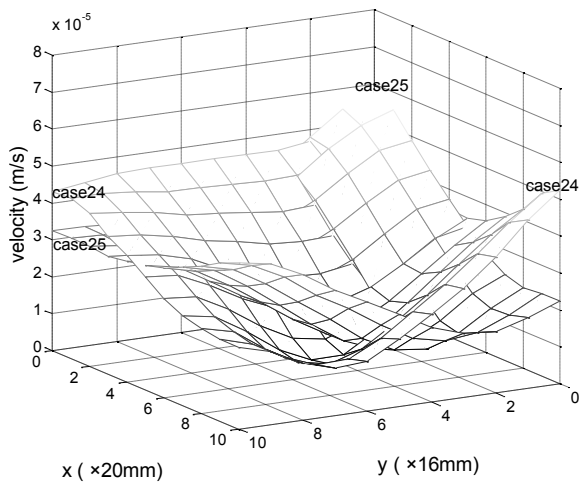
(d)



(b)



(e)



(c)

**Figure 13:** Vibration distribution on the winding at 100 Hz for severely loosened cases, Cases 22–28.

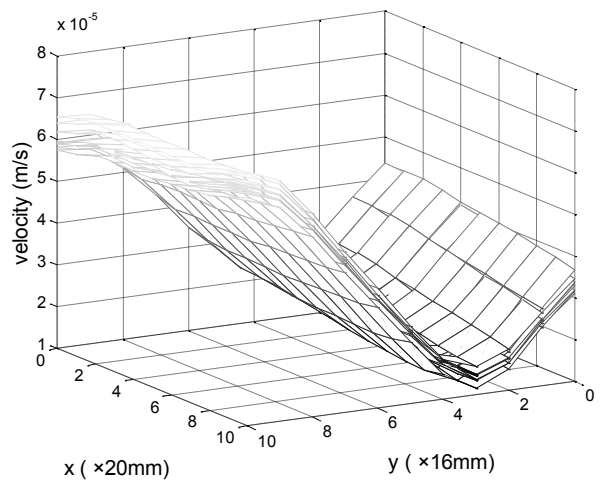


**Figure 14:** Vibration distribution on the winding at 100 Hz for totally loosened cases, Cases 29–36.

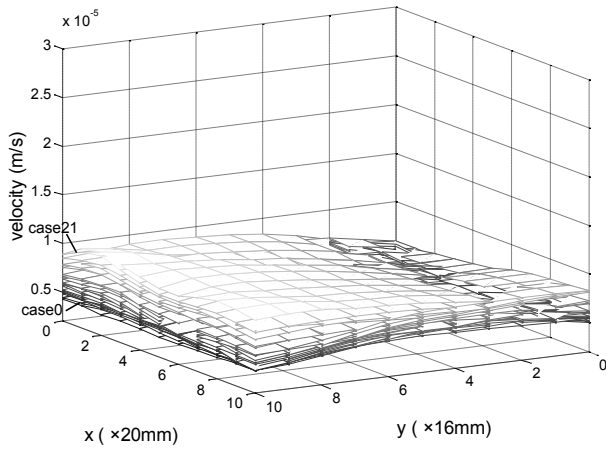


**Figure 15:** Vibration distribution on the winding at 200 Hz for Cases 0–21.

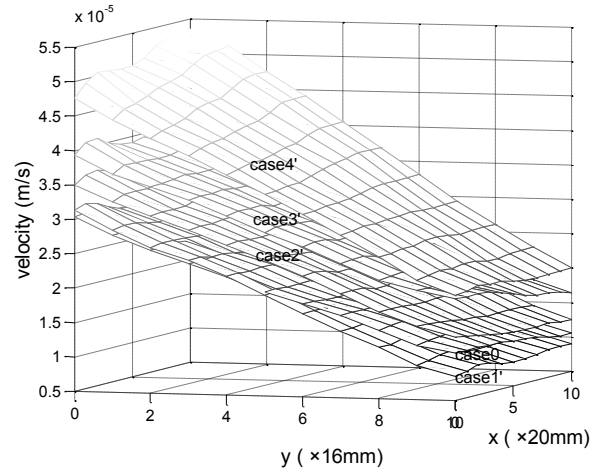


**Figure 18:** Vibration distribution on the winding at 100 Hz for Cases 0, 1'–4'.

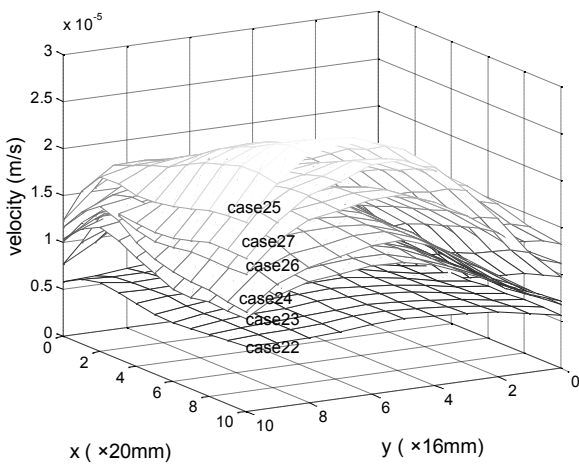


**Figure 16:** Vibration distribution on the winding at 200 Hz for Cases 22–27.

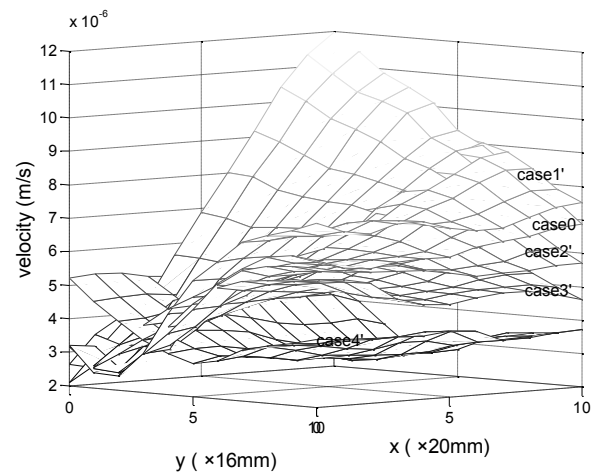


**Figure 19:** Vibration distribution on the winding at 200 Hz for Cases 0, 1'–4'.

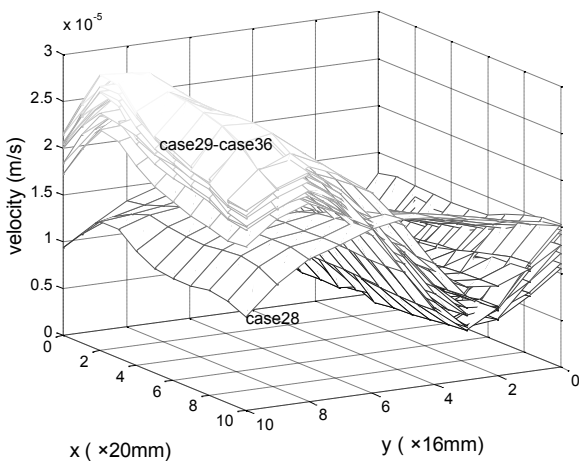


**Figure 17:** Vibration distribution on the winding at 200 Hz for Cases 28–36.

**Case 1' to Case 4'**

Removal of the insulation blocks also introduced local changes to the winding structure. As shown in Figures 18 and 19, removing the blocks (Cases 1'–4') leads to a rise in vibration amplitudes at all scanning points at 100 Hz, and a fall in amplitudes at 200 Hz. Notwithstanding the obvious increase in 100 Hz vibration, the pattern of velocity distribution at 100 Hz stays almost unchanged. However, the 200 Hz vibration begins to perform differently to that at 100 Hz. When more than three blocks are removed, the pattern of the velocity at 200 Hz is totally different from that of Case 0. This observation indicates that the velocity patterns at higher frequencies are more sensitive to local changes in the winding.

In summary, the velocity distribution  $S(f)$  at the dominant frequencies is sensitive to structural changes introduced by the two failure modes discussed above. The characteristics of  $S(f)$  vary with the level of failure severity.

To describe the variance of the difference between the velocity distributions  $S_A(f)$  and  $S_0(f)$ , the spatial variance of the distributed winding velocity for each case with respect to Case 0 (the healthy winding) is defined as:

$$\alpha_i(f) = \frac{\sum_{n=1}^{11} \sum_{m=1}^{11} (\Delta S_{n,m,i}(f) - \overline{\Delta S_i}(f))^2}{11 \times 11}, \quad (3)$$

where:

$$\overline{\Delta S_i}(f) = \frac{\sum_{n=1}^{11} \sum_{m=1}^{11} \Delta S_{n,m,i}(f)}{11 \times 11}, \quad (4)$$

$$\Delta S_i(f) = S_i(f) - S_0(f) = \begin{bmatrix} \Delta S_{1,1,i}(f) & \dots & s_{i,1}(f) \\ \vdots & \ddots & \vdots \\ \Delta S_{11,1,i}(f) & \dots & s_{i,11}(f) \end{bmatrix} \quad (5)$$

and  $N$  is the number of cases.

In Figures 20 and 21,  $\alpha(100)$  and  $\alpha(200)$  both increase with the looseness of clamping pressure, but the former is more sensitive. Moreover, Figures 22 and 23 indicate that local changes, even slight ones, will also result in a variation of the velocity distribution at the dominant frequencies. However, it is obvious that  $\alpha(200)$  is a more sensitive and accurate approach to the detection and identification of local changes in the structure of the winding.

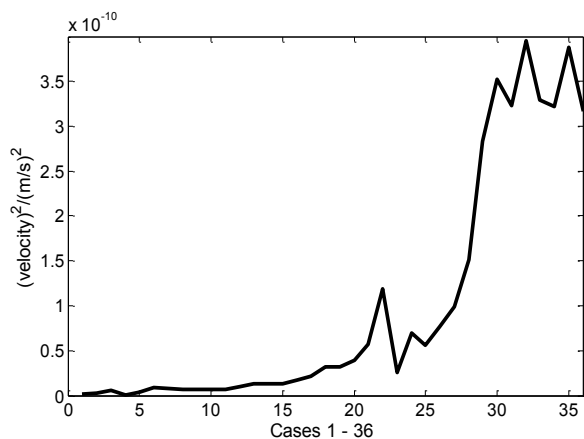


Figure 20: Spatial variance  $\alpha(100)$  for Cases 1 to 36.

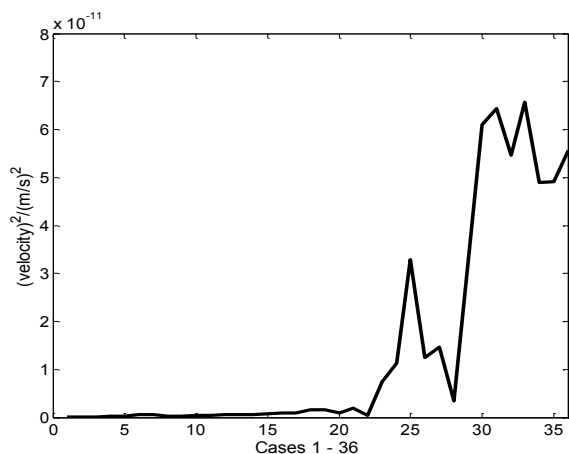


Figure 21: Spatial variance  $\alpha(200)$  for Cases 1 to 36.

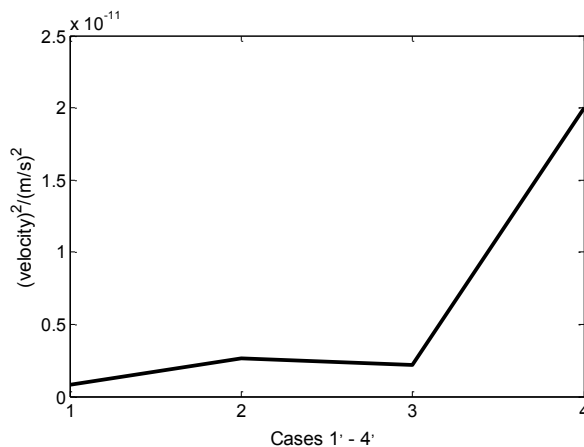


Figure 22: Spatial variance  $\alpha(100)$  for Cases 1' to 4'.

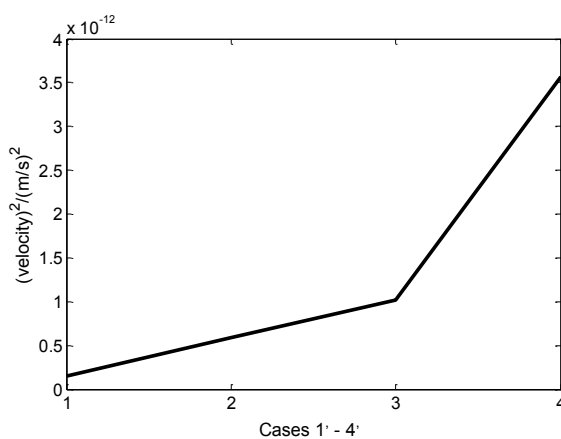


Figure 23: Spatial variance  $\alpha(200)$  for Cases 1' to 4'.

### CONCLUSION

Detailed measurements of winding vibration were performed on a single-phase transformer. Some results can be summarized as follows:

- (1) A laser scanning technique allowed a high spatial resolution for 3D co-ordinate measurements, which gave rise to a detailed and refined vibration pattern across the testing surface of the transformer winding.
- (2) The vibration patterns depended heavily on the overall health of the winding structure. When the transformer was operating in a healthy condition, the velocity distribution on the winding at 100 Hz followed a pattern with an approximate bilateral (left-right) symmetry across the horizontal axis and an apparent linear decrease along the vertical axis. Once a fault was introduced, the velocity pattern altered in consequence.
- (3) Individual faults produced their own characteristic vibration patterns at the dominant frequencies. The spatial variance was used to describe the variance of the difference between the velocity distributions  $S_i(f)$  and  $S_0(f)$ , which turned out to be a sensitive and accurate measure of the winding faults.

In conclusion, a laser-based measurement of winding vibration has provided greater insight into the winding's vibration characteristics in relation to different mechanical properties

of the winding. Changes in those properties often corresponded to the causes of failure in the transformer winding.

External measurements, which are non-invasive and convenient, are preferred in on-line condition monitoring and fault diagnosis systems. As such, most vibration measurements of power transformers are performed externally, utilizing the vibration signature of the transformer tank to identify the health conditions of the active part within a transformer. However, there is still a lack of understanding of the relationship between internal and external measurements. A better understanding and complementation between these two measurements will improve the reliability and efficiency of a vibration-based condition monitoring system, which will be an ongoing effort in this research project.

## ACKNOWLEDGMENTS

The first author is thankful for the financial support from the China Scholarship Council (CSC). The financial support for the UWA transformer project by the CRC for Infrastructure Engineering Asset Management (CIEAM) is also gratefully acknowledged.

## REFERENCES

- Lord, T & Hodge, G 2010, '*Interfacing on-line monitoring technologies to power transformers*', Lord Consulting. <<http://www.lordconsulting.com/images/stories/pdf/Transformer-Monitoring-jul10.pdf>>.
- Bagheri, M & Naderi, MS 2011, '*On-line transformer winding deformation diagnosis: a profound insight to methods*', 26<sup>th</sup> International Power System Conference, Tehran, Iran, pp. 1–14.
- Berler, Z et al 2000, '*Vibro-acoustic method of transformer clamping pressure monitoring*', Conference Record of the 2000 IEEE International Symposium on Electrical Insulation, Anaheim, USA, pp. 263–266.
- Nafar, M, Bahmanifirouzi, B & Jabbari, M 2011, '*Transformer monitoring by using vibration analysis*', Australian Journal of Basic and Applied Sciences, vol. 5, no. 11, pp. 984–990.
- Bartoletti, C et al 2004, '*Vibro-acoustic techniques to diagnose power transformers*', IEEE Transactions on Power Delivery, vol. 19, no. 1, pp. 221–229.
- Shengchang, J et al 2001, '*The vibration measuring system for monitoring core and winding condition of power transformer*', Proceedings of 2001 International Symposium on Electrical Insulating Materials, Himeji, Japan, pp. 849–852.
- Borucki, S 2009, '*Vibroacoustic Measurements in a Transient State of Transformer Operation*', Optical and Acoustical Methods in Science and Technology, vol. 116, no. 3, pp. 277–280.
- Boczar, T & Borucki, S 2008, '*The analysis of mechanical vibrations and acoustic pressure level of a transformer model*', Optical and Acoustical Methods in Science and Technology, vol. 114, no. 6-A, pp. A21–A25.
- Bel'en, G & Juan, CB 2005, '*Winding deformations detection in power transformers by tank vibrations monitoring*', Electric Power Systems Research, no. 74, pp. 129–138.
- Miguel, A & Sanz, B 1997, '*Experiences learned from the on-line internal monitoring of the behaviour of a transformer*', Electric Machines and Drives Conference Record, Milwaukee, USA, pp. TC3-11.1 – 11.3.
- Ming, J & Jie, P 2010, '*A study of vibration properties of parallel beams coupled by insulation elements*', Australasian Congress on Applied Mechanics, Perth, Australia, pp. 520–531.
- Pan, J, Jin, M & Wang, Y 2011, '*Vibration of power transformers and its application for condition monitoring*', The 14<sup>th</sup> Asia Pacific Vibration Conference, Hong Kong, China, 1, pp. 84–93.
- Mizokami, M, Yabumoto, M & Okazaki, Y 2005, '*Vibration analysis of a 3-phase model transformer core*', Electrical Engineering in Japan, vol. 119, no. 1, pp. 1–8.
- Dey, D & Chakravorti, S 2011, '*Cross-correlation aided wavelet network for classification of dynamic insulation failures in transformer winding during impulse test*', Dielectrics and Electrical Insulation, vol. 18, no. 2, pp. 521–532.
- Oliveira, LMR & Cardoso, AJM 2010, '*Power transformers behavior under the occurrence of inrush currents and turn-to-turn winding insulation faults*', Electrical Machines, 2010 XIX International Conference on, Rome, Italy, pp. 1–7.